Modeling Nano-Sized Single Molecule Objects: Dendronized Polymers Adsorbed onto Mica

Oscar Bertran,[a,*] Baozhong Zhang,[b] A. Dieter Schlüter, [c] Martin Kröger,[c] and Carlos Alemán[d,e,*]

[a] Departament de Física Aplicada, Escola d'Enginyeria d'Igualada, Universitat Politècnica de Catalunya, Pça Rei 15, Igualada 08700, Spain

[b] Center of Analysis and Synthesis, Lund University, P.O. Box 124, SE-22100 Lund, Sweden

[c] Department of Materials, Institute of Polymers, Swiss Federal Institute of Technology, ETH Zurich, HCI J 541, 8093 Zurich, Switzerland

[d] Departament d'Enginyeria Química, E. T. S. d'Enginyeria Industrial de Barcelona, Universitat Politècnica de Catalunya, Diagonal 647, Barcelona E-08028, Spain

[e] Centre for Research in Nano-Engineering, Universitat Politècnica de Catalunya, Edifici C', C/Pasqual i Vila s/n, Barcelona E-08028, Spain

[*] Corresponding authors:

O.B. Departament de Física Aplicada, Escola d'Enginyeria d'Igualada, Universitat Politècnica de Catalunya, Pça Rei 15, Igualada 08700, Spain. Phone: +34 – 938035300. Mail: oscar.bertran@upc.edu

C.A. Departament d'Enginyeria Química, E. T. S. d'Enginyeria Industrial de Barcelona, Universitat Politècnica de Catalunya, Diagonal 647, Barcelona E-08028, Spain. Phone: +34 – 934010883. Mail: carlos.aleman@upc.edu

ABSTRACT

In this work we attempt to provide direct evidence for the suggested behavior of dendronized polymers as molecular objects (*i.e.* single shape persistent macromolecules). For this purpose, the microscopic structure of dendronized polymers adsorbed onto mica has been investigated using atomistic molecular dynamics simulations. We find that the shape of the second to fourth generation dendronized polymers is basically kept upon adsorption due to substantial *backfolding* within their interior. The fluctuation strength of the polymer backbones, which is seen to decrease with increasing generation, also indicates that these individual macromolecules exhibit molecular object behavior in the nano size range.

KEYWORDS: Backfolding; Circularity; Cylindrical molecules; Dendrimer; Molecular dynamics; Persistent shape

INTRODUCTION

Dendronized polymers (DPs) are hyperbranched macromolecules that possess a linear main chain and dendron-type side chains (*i.e.* repetitively branched side chains).[1-3] Steric repulsions among neighboring dendrons, increasing in strength with the dendrons generation number, *g*, compel polymer main chains to extend from random coils to bendable rod-like cylinders. This behavior is completely different from that of dendrimers, which typically adopt a spherical shape because all dendrons are attached to a central core). Consequently, the interactions between neighboring dendrons are much less repulsive for dendrimers than for DPs and, therefore, the maximum generation (g_{max}) allowed for the former is significantly higher than for the latter.

The rigidity, cross-sectional diameter, number of functionalities per backbone unit length and properties of DPs can be controlled by altering *g*.[2,4] DPs, which are considered as nano-sized single molecular objects[5] with functional surfaces (*i.e.* DPs bear a large and defined number of functionalized groups in the outer shell due to their hyperbranched nature),[6-9] have attracted great attention as an emerging class of nanomaterials to stabilize therapeutic proteins in the gastrointestinal tract,[10] to catalyze reactions,[11] and both copy[12] and immobilize enzymes.[13]

The structure of a homologous series of neutral DPs composed of a poly(methacrylic acid) backbone, whose repeat units are regularly branched dendrons of generation *g* containing both amide and aromatic groups (Scheme 1), was investigated at the nanometer level by atomic force microscopy (AFM) and transmission electron microscopy (TEM)[2-4] and at the atomistic level using molecular dynamics (MD) simulations.[14,15] AFM and TEM studies of DPs adsorbed onto attractive mica surfaces were found to exhibit the scaling behavior of a compact cylinder, which was also evidenced by MD simulations.

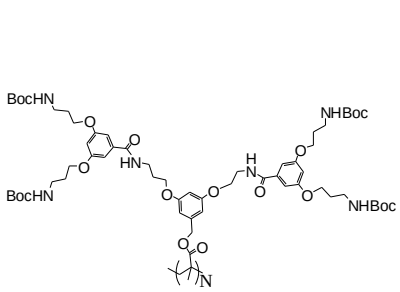

PG2

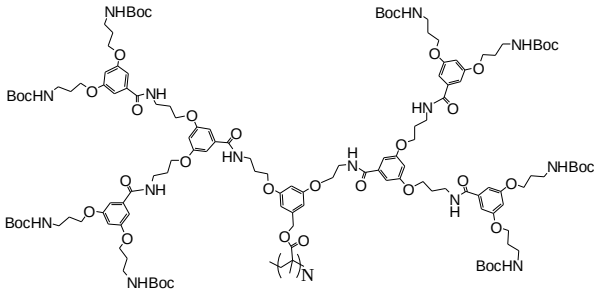

PG3

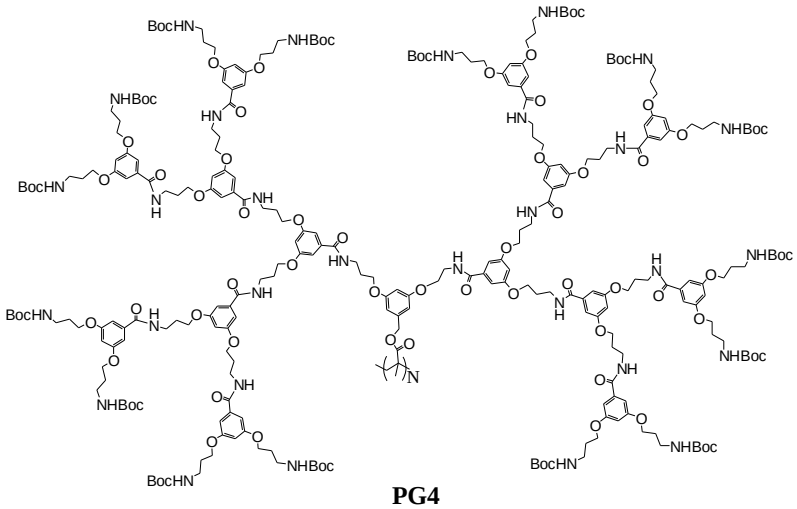

PG4

Scheme 1. Chemical structures of PG2-PG4: the sub-index *N* at the parenthesis in the linear main chain refers to the number of repeat units while the Boc at the outer shell of the repeat unit refers to *tert*-butyloxycarbonyl protecting group.

The apparent height of DPs adsorbed onto mica, as measured by TEM (h^{TEM}),[2-4] was systematically smaller than the cross-sectional diameter predicted by MD (D^{MD}) for the same systems in an isotropic environment,[14,15] the difference D^{MD}–h^{TEM} increasing with *g*. This feature, which is experimentally supported by the visual impression that DPs adsorb as deformed cylinders,[2-4] suggested that the dimensions of this particular class of macromolecules are affected by surface···polymer interactions. On the other hand, some of us recently proved that DPs belonging to this homologous series behave as molecular objects (*i.e.* single shape persistent macromolecules), retaining approximately their form

and mesoscopic dimensions irrespective of solvent quality and adsorption onto a surface.[5] This was fully consistent with the fact that DPs are dominated by intramolecular interactions. Indeed, in a very recent study devoted to examine the interaction between several macromolecular chains, we found that the role of intermolecular interactions on the mean DP diameter and surface roughness is negligible.[16]

As the influence of the surface···polymer interactions in the deformability and behavior as molecular object of DPs is not completely understood at the microscopic level, in this work we have examined the effect of a solid substrate on the molecular structure of DPs. More specifically, the molecular dimensions and internal organization of DPs with *g* ranging from 2 to 4 (abbreviated PG2-PG4; Scheme 1) adsorbed onto mica have been investigated using atomistic MD. This study aims at substantiating the aspect whether or not particularly high *g* DPs qualify as linear molecular objects and thus intermediate entities between common polymer chains and colloidal particles. Furthermore, results have been also used to clarify the boundary between deformed and molecular objects, which is indeterminate at present time.

THEORETICAL METHODS

The structure of PG2-PG4 (Scheme 1) has been investigated in the free-state (PGg^{free}) and adsorbed onto mica (PGg^{mica}) considering a macromolecules containing 150 repeat units. This represents a total of 27148, 57748 and 118948 explicit atoms for PG2, PG3 and PG4 molecules, respectively. Simulations of PGg^{free} were performed in vacuum, such solvent-free case reflecting the situation encountered in poor solvents. This was recently corroborated by comparing results derived from vacuum conditions with those obtained in chloroform solution, where the DPs swell ("good solvent").[14]

Simulations of PGg^{mica} were performed putting a DP molecule onto a mica surface. No solvent was considered above the surface to reflect the situation encountered in the microscopy experiments.[17] All PGg^{mica} simulations were performed applying periodic boundary conditions to an orthorhombic simulation box of a= 310 Å, b= 322 Å and c= 490 Å. It should be noted that the extension of the box in the z-direction is much larger than the extension of the system, leaving the system effectively periodic in the x- and y-directions.

Molecular models obtained in our previous work[14] for PG2-PG4 were used as starting point of the current simulations. For PGg^{free} the system temperature was heating up from 0 to 298 K using a rate of 1 K each 1.5 ps. After this, production runs of 20 ns were started. For PGg^{mica} simulations, the molecular models were put above (parallel) the mica surface at a distance of ~15 Å. After this, the potential energy of each system was minimized for 5000 steps using the conjugate gradient algorithm. Next, each DP-surface system was submitted to 1 ns of NVT MD at 50 K. This run led to the deposition of the DP on the mica surface. Then, all atoms of each system were submitted to 2 ns of steady heating until the target temperature was reached (298 K) followed by 1 ns of thermal equilibration. Finally, 20 ns of NVT MD simulations were carried out for production.

MD simulations of PGg^{free} and PGg^{mica} were performed using the NAMD program.[18] The energy was calculated using the AMBER force-field,[19] all the bonding and van der Waals parameters required for the DPs under study being taken from Generalized AMBER force-field (GAFF).[20] Atomic charges were extracted from a previous electrostatic parametrization of these systems. The mica $K_{1.0}[Si_3Al_1O_8][Al_2O_2(OH)_2]$ surface was represented using the force-field parameters reported by Heinz and co-workers.[21] The unit cell dimensions provided by such parameters for this dioctahedral

phyllosilicate are *a*= 2.585 Å, *b*= 2.690 Å, *c*= 2.004 Å, α=89.4º, β= 95.3º and γ= 90.1º, which are very close to the experimental ones (*i.e.* *a*= 2.596 Å, *b*= 2.705 Å, *c*= 2.005 Å, α= γ= 90º and β= 95.7º).[22] The mica super cell model constructed in reference 21 was kindly supplied by Dr. Heinz and adapted to the dimensions of the simulation box. The thickness *(i.e.* extension in the *c*-direction) of this sheet model was 6.7 Å. In order to avoid the bending of the mica sheet during the MD simulations, the position of the oxygen atoms located at the lowest part of the surface was kept fixed in the *z*-direction during the simulations (*i.e.* displacements for such atoms were allowed in the *x*- and *y*-directions only).

Atom-pair distance cut-offs were applied at 12 A to compute van der Waals and the Ewald direct sum electrostatic interactions. The Ewald reciprocal sum electrostatic interactions were calculated using Particle Mesh Ewald (PME) with a points grid density of the reciprocal space of 1 $Å^3$.[23] Bond lengths involving hydrogen atoms were constrained using the SHAKE algorithm with a numerical integration step of 2 fs.[24] The nonbonded pair list was updated every 5 steps. Coordinates of all the production runs were saved every 25000 steps (50 ps intervals, 400 snapshots in total) for subsequent analysis. Structural parameters were averaged considering the snapshots recorded during the last 10 ns.

RESULTS AND DISCUSSION

Models obtained for these polymers[14] have been used to construct initial geometries for the DPs adsorbed onto an attractive mica surface (PGg^{mica}), which were used as starting point of 20 ns MD runs. For comparison, additional 20 ns long MD runs were performed using the surface-free DPs (PGg^{free}). Inspection of the temporal evolution of different structural parameters, as for example the end-to-end distance (L_{ee}) and the

radius of gyration (R_g), indicates that the structure of all the studied systems is equilibrated and relaxed (Figure S1). On the other hand, Figure 1 evidences adsorption-induced flattening of PG2-PG4 as obtained from MD simulations.

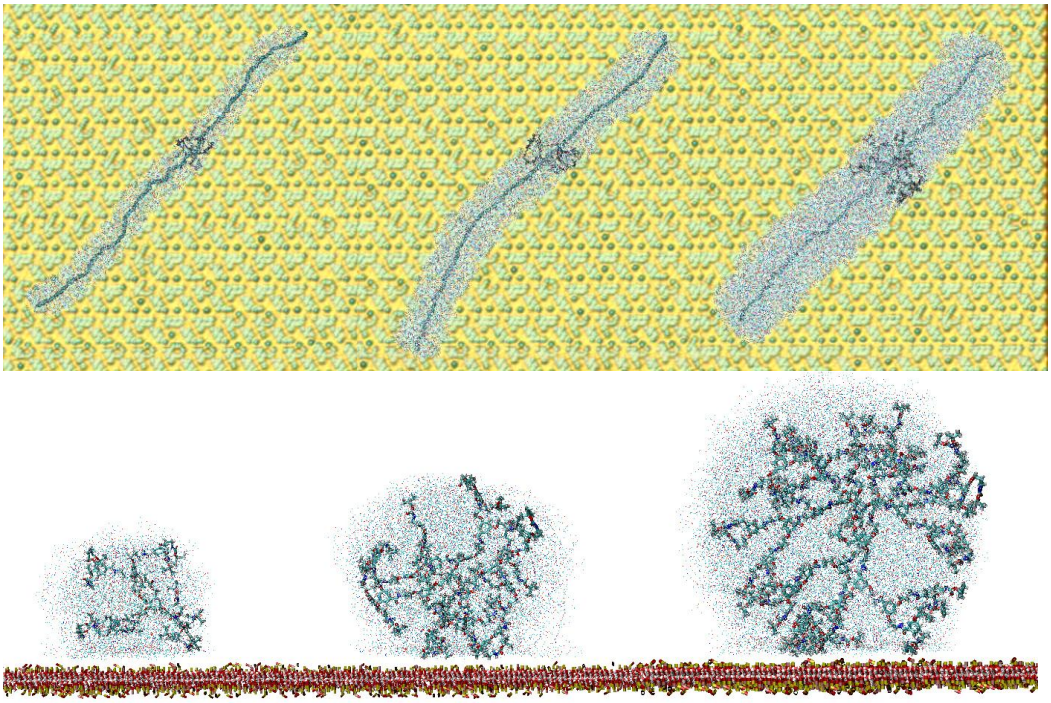

Figure 1. Axial (top) and equatorial (bottom) views of PG2 (left), PG3 (middle) and PG4 (right) adsorbed onto mica after 20 ns MD. To clarify the representation only four branched dendrons are explicitly depicted for each system.

DPs in the unperturbed state have strictly circular cross-sections. The degree of deformability has been quantified by comparing the cross-sectional heights and widths of molecules adsorbed onto mica (h^{MD} and w^{MD}), as derived from the distributions of the DP mass as a function of the radial distance (*i.e.* perpendicular to the surface) and of the axial distance (*i.e.* parallel to the surface) from the center of mass of the polymer chain, respectively. These distributions, which are displayed in Figure 2, were obtained by averaging over 300 snapshots taken during the last 15 ns of the 20 ns MD production runs. For each DP,h^{MD} and w^{MD} were estimated as the distance at which the radial and

axial mass profiles had dropped to 50% of their maximum values before reaching the external layer of the DP, values being listed in Table 1.

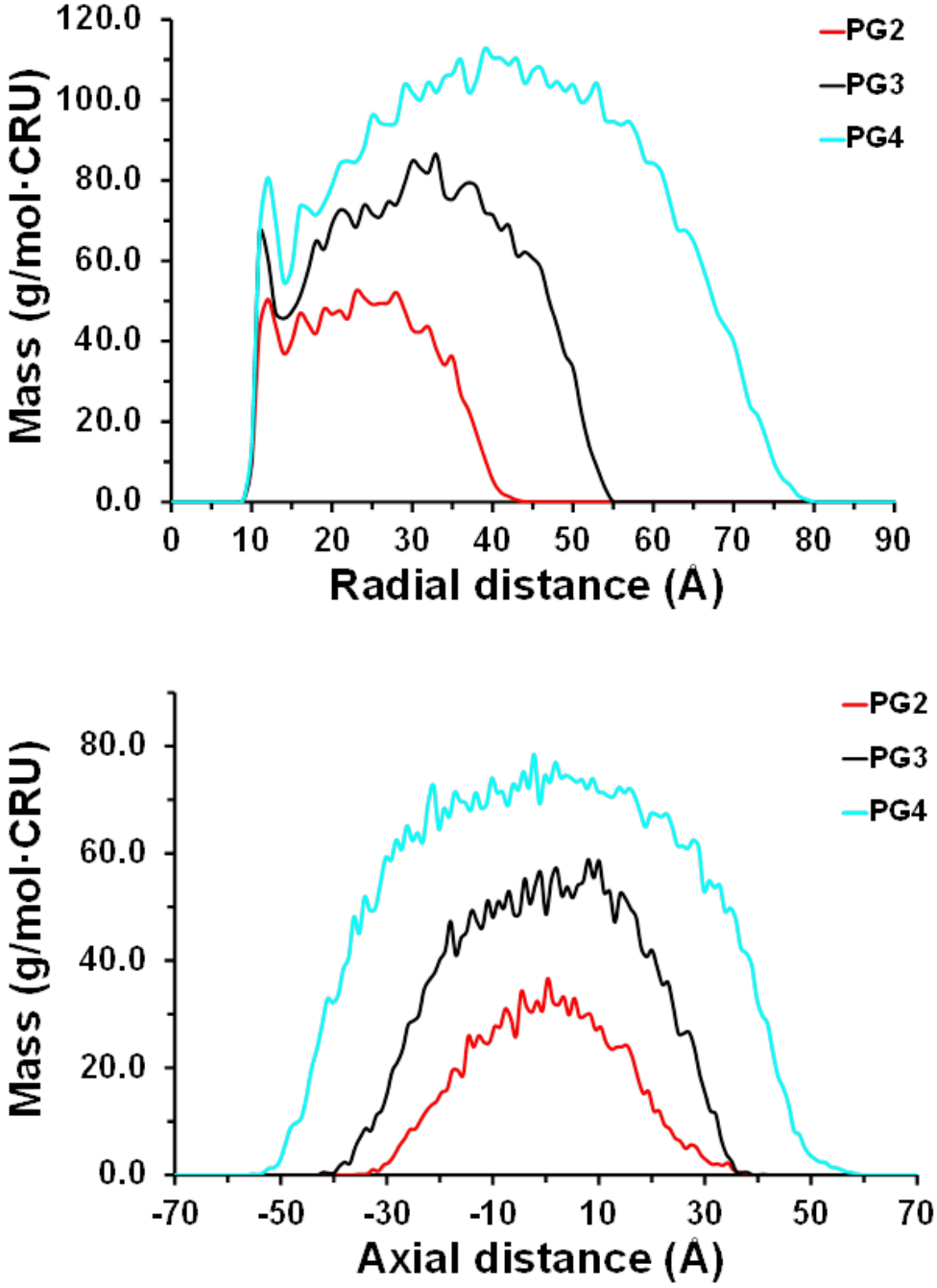

Figure 2. Distribution of DP mass deposited on mica as a function of the (a) radial and (b) axial distance (*i.e.* perpendicular and parallel to the mica surface, respectively) from the center of mass of the polymer chain.

Table 1. Height (*h*; in Å) and Width (*w*; in Å) Determined for PGg^{mica} using MD Simulations and Experimental Techniques, and Diameter (*D*; in Å) Derived from MD Simulations for PGg^{free}.

	PG2	**PG3**	**PG4**
h^{MD} **(calc. MD adsorbed on mica)**	27.1	35.0	57.5
w^{MD} **(calc. MD adsorbed on mica)**	33.9	48.0	73.6
h^{TEM} **(exp. TEM adsorbed on mica)**	23±4	34±5	49±3
w^{SEM} **(exp. SEM adsorbed on mica)**	31±4	45±4	60±4
D^{MD} **(calc. MD free state)**	34.4	49	71.8

The graphical representation of h^{MD} against w^{MD} (Figure 3a) reflects that the latter is ~30% larger than the former, irrespective of *g*, highlighting the deformation undergone by DPs upon adsorption onto the attractive solid surface. This deformation is significantly lower than that typically reported for dendrimers, which frequently exceed 100% for *g* similar to those studied in this work (detailed discussion of this feature is provided below).[25,26]

The variation of both h^{MD} and w^{MD} against *g* suggests an exponential behavior (Figure 3b). The latter is consistent with the organization of the outermost branching units (*i.e.* external dendrons) when *g* grows from 3 to 4,[14] which affects the stiffness of the macromolecular backbone and the effective strength of inter-dendron interactions. Thus, the internal packing of external dendrons is higher in terms of alignment of their terminal strands for $g \geq 4$ than for $g < 4$. This alignment, which is due to the particular architecture of DPs, is mainly provoked by a looping or "*backfolding*" phenomenon (*i.e.* external dendrons approach and surround the macromolecular backbone) that occurs for $g \geq 4$.

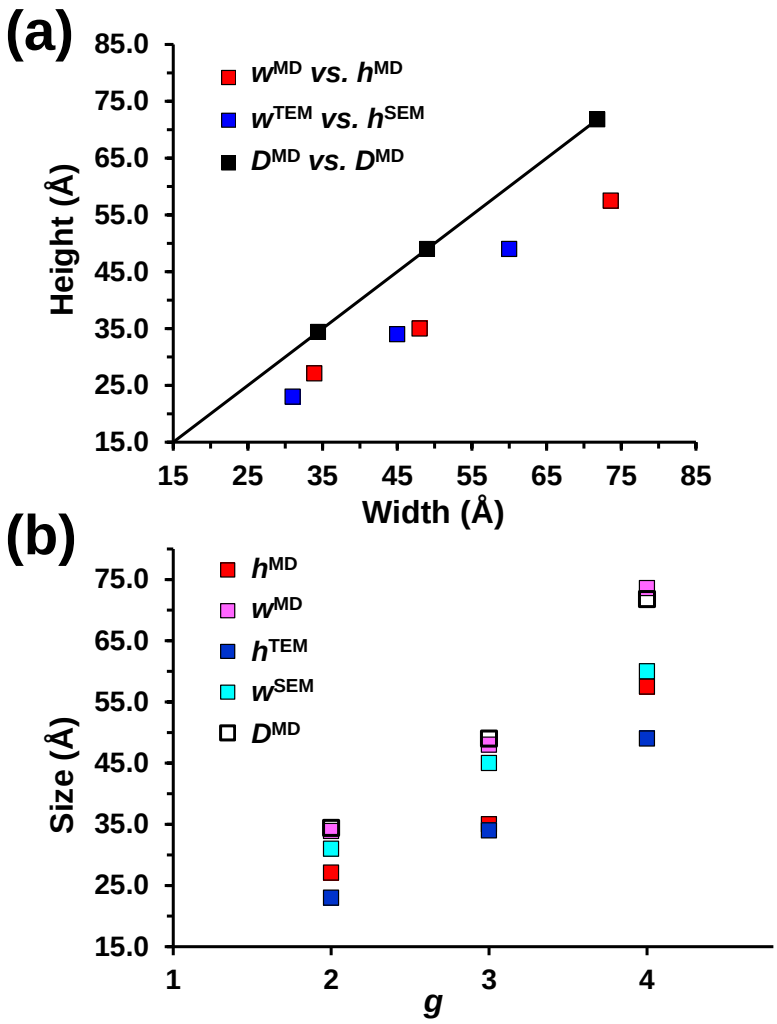

Figure 3. (a) Representation of the width against the height estimated for PGg^{mica} using MD and experimental techniques. Black diagonal and squares correspond to the radii estimated from PGg^{free} simulations. (b) Height, width and radii against the generation number g.

Simulations of PGg^{free} led to non-deformed cylindrical structures. The radial density profiles, $\rho(r)$, measured using the vector perpendicular to the molecular axis, indicate that the density is maximal in the vicinity of the backbone and dropping rapidly to a value of ~1.1 g/cm^3 as the distance to the backbone increases, independently of g (Figure S2). Over a range of distances the density remains approximately constant up to the length of the partially extended g-generation strand, where $\rho(r)$ approaches zero.

Assuming a homogeneous cylinder, the D^{MD} values derived from the $\rho(r)$ profiles, defining the straight line in the diagonal of Figure 3a, corroborate the deformation of the DPs. Thus, D^{MD} values are similar to w^{MD} and larger than h^{MD} (Figure 3b), the difference D^{MD}–h^{MD} increasing from 7.3 to 14.3 Å when g grows from 2 to 4. The D^{MD} predicted in this work using the last 15 ns of 20 ns long MD simulations are very similar to those previously obtained using the last 1 ns of 10 ns long MD runs (*i.e.* deviations ≤ 1.2%).[14] On the other hand, as occurred for the width, the average length is not altered by the mica surface (Table S1). These analyses clearly indicate that deposition of DPs onto solid surfaces only provokes 1D-deformations.

The electrostatic and van der Waals component of the interaction energy have been evaluated by accounting the interactions between the atoms at the inorganic surface and the atoms belonging to the adsorbed DPs (Table S2). Data were obtained by averaging over 300 snapshots taken during the last 15 ns of the 20 ns MD run for PGg^{mica}. The total interaction energy (E_{TOT}) rapidly decreases with increasing g, evidencing the attraction exerted by the mica surface towards the DPs. As it was expected, this stabilization is mainly due to the electrostatic interactions, which represent about 75% of E_{TOT}. Despite of the predominance of the electrostatic contribution, the role of the van der Waals interactions should not be considered as negligible. These interactions become around 20-30% more attractive for each increment of g.

Experimental estimations of the dimensions of PG2-PG4 deposited onto mica were obtained using different techniques. The height and width values determined by TEM and scanning electron microscopy (SEM), respectively, are in very good agreement with the theoretical estimations provided in this work ($h^{MD} \approx h^{TEM}$ and $w^{MD} \approx w^{SEM}$ in Figure 3b). Thus, the slight overestimation of h^{MD} and w^{MD} should be essentially attributed to the arbitrary definition of these parameters. Importantly, representation of h^{MD} *vs.* w^{MD}

and h^{TEM} *vs.* w^{SEM} shows the same behavior (Figure 3a), h^{MD}/w^{MD} and h^{TEM}/w^{SEM} being around 0.7-0.8 for the range of *g*'s studied.

Although Figure 1 qualitatively describes the deformation caused by the mica surface on the cylindrical models of PG2-PG4, a quantitative estimation has been obtained by comparing the cross-section circularities of PGg^{mica} and PGg^{free}. To this end, solid images of the sections (equatorial projections) of each model were constructed (Figure 4) for subsequent analysis. Other representative solid images of the section of the models obtained for PG2-PG4 adsorbed onto mica and in the free-state are displayed in Supporting Information (Figures S3 and S4).

The cross-section circularity (*C*) of such two-dimensional shapes was calculated via:

$$C = 4\pi A / P^2 \qquad (1)$$

where *A* and *P* refer to the area and perimeter, respectively, obtained by counting the pixels of the different images. Obviously, in all cases *C* is higher for PGg^{free} than for PGg^{mica}, while the loss of circularity is only $\Delta C = 1.8\pm0.2$, 3.0 ± 0.3 and $7.7\pm0.2\%$ for PG2, PG3 and PG4, respectively. It should be noted that ΔC involves two contributions: the mica-induced shape deformation and the small surface protuberances associated to the organization of the dendrons at the periphery of cylindrical cross section. This result suggests that the loss of circularity of PG(*g*+1) increases twice with respect to PG*g* for the investigated range of *g* that clearly remains below a maximum generation caused by packing constraints.

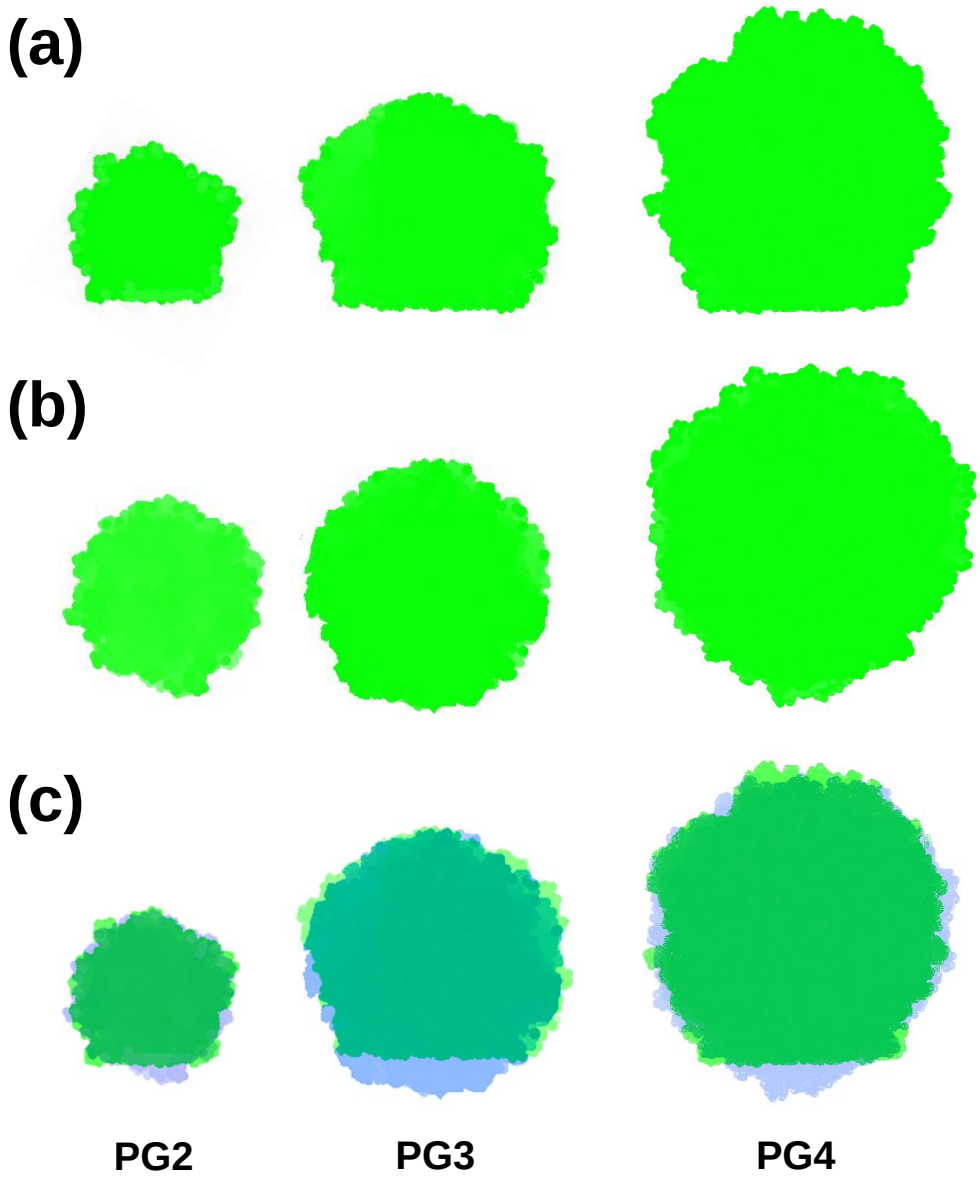

Figure 4. Solid images of the section (equatorial projection) of the models obtained for PG2-PG4 (a) adsorbed onto mica and (b) in the free-state. The superposition of the sections displayed in (a) and (b) is provided in (c).

The relatively small deformation of DPs in PGg^{mica} is evidenced by comparing the density profiles representing the density (r) against the distance r along the cross-sectional section for PGg^{free} and from the surface to the cross-sectional height for PGg^{mica} (Figure 5). This graphic clearly reflects that the relative flattening of PGg upon

deposition on to the mica surface decreases with g. These results are fully consistent with the solid images of the section provided in Figures 4, S3 and S4.

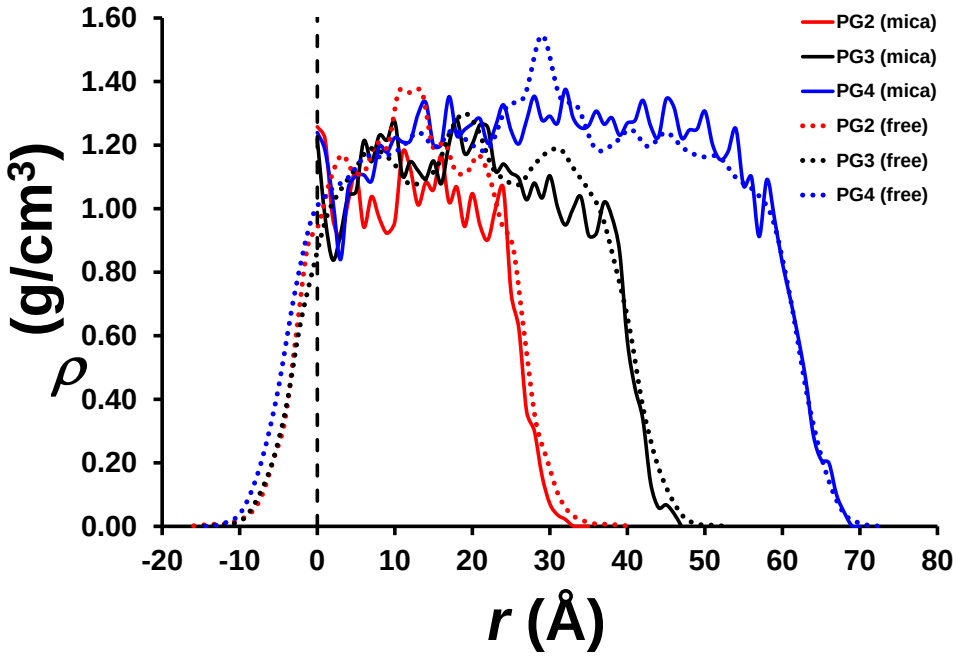

Figure 5. Representation of the density (r) against the distance r along the cross-sectional section for PGg^{free} and from the surface to the cross-sectional height for PGg^{mica}. The profile displayed for each DP corresponds to an average considering different cross-sections within a given snapshot. Data were obtained by averaging over snapshots taken during the last 15 ns of the 20 ns MD run. The position of the surface is indicated by the dashed lines.

Figure 6 depicts the radial probability distribution function of the *tert*-butyloxycarbonyl (Boc) groups located at the ends of each external dendron as a function of the distance of the macromolecular backbone, $g_{\text{Boc-b}}(r)$, for PGg^{free} and PGg^{mica}. The peak obtained for PG2, PG3 and PG4 in the free-state, which becomes smaller and broader with increasing g, is centred at $r\approx$ 15, 23 and 35 Å, respectively. The most striking result, however, is the broad inner $g_{\text{Boc-b}}(r)$ tail as it also grows with g. The fact that $g_{\text{Boc-b}}(r)$ is non-zero at distances much smaller than the radius of the DP

reflects backfolding, which becomes more pronounced with increasing *g*. Such backfolding seems to imply a reduction of the mobility of the whole system (*i.e.* backbone and side groups). The $g_{\text{Boc-b}}(r)$ profiles of PGg^{mica} are consistent with an increment of the backfolding, which is especially evident for PG4. Thus, the main peaks shift towards smaller *r* values, now being centred at $r \approx$ 13, 20 (with a second peak at 25 Å) and 32 Å for PG2, PG3 and PG4, respectively. The surface-induced increment of the backfolding, which we estimated from $g_{\text{Boc-b}}(r)$ profiles, increases from 7.1% (PG2) to 9.5% (PG4). Although the number of Boc groups occupying inner regions is higher for PGg^{mica} than for PGg^{free}, the amount of Boc groups immediately next to the backbone remains unaffected. The conformational restrictions associated with the dendronized architecture preclude any enhancement of the backbone wrapping phenomenon at the most internal region. The DP shape is kept regardless of the attractive forces induced by the mica surface.

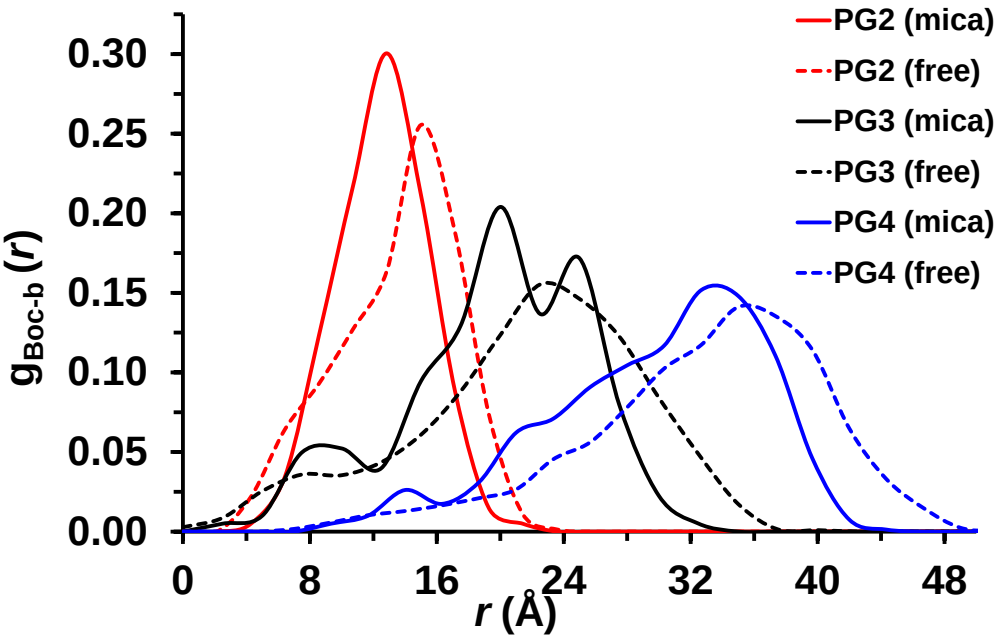

Figure 6. Distribution of Boc groups ($g_{\text{Boc-b}}$) for PGg^{free} and PGg^{mica}.

It should be noted that the amount of backfolding and surface-induced deformability have been also studied for (polyamidoamine) dendrimers.[25] However, the properties of dendrimers, which can be defined as monodisperse and usually highly symmetric spherical compounds (*i.e.* dendrons are linked to a single core unit rather than to a linear main chain like in DPs), cannot be directly compared with those of DPs unless the formers reach a dense packing state through g_{max}.[26]

The polymeric backbone plays a crucial role in the steric congestion and molecular strain observed in DPs with g well below the packing limit, g_{max}, while for dendrimers no such mechanism is at work.[25,26] Accordingly, the surface induced flatting is higher for dendrimers than for DPs at $g < g_{max}$. Indeed, computer simulations of DPs with a relatively low number of repeat units (*i.e.* 25-30) show end cap effects (results not shown) that resemble the deformability of dendrimers adsorbed on surfaces. In these DPs dendrons located at the two ends tend to use the available space and the hemispherical end caps to align in the direction of the macromolecular backbone, whereas in adsorbed dendrimers at low g dendrons tend to occupy the spherical free volume around the core[17] to form very flat structures. The observartions that dendrimers flatten more than DPs with identical number of generations is consistent with the fact that $g_{max} < 7$ for DPs[4,14] while $g_{max} \approx 12$ for a typical dendrimer.[31] Thus, the DPs studied in this work (g= 2-4) are closer to a DP at g_{max} than dendrimers with the same g to a dendrimer at g_{max}.

The impact of both mica and g on the rigidity of DPs has been estimated using the inverse variance of the end-to-end distance (L_{ee}) distribution, $\overline{L_{ee}^2} - (L_{ee})^2$, which describes the rigidity along the helical backbone axis. Independently of g, the inverse variance is smaller for PGg^{free} than PGg^{mica} (Figure 7), indicating that the behavior as helical rigid rod is enhanced in the latter with respect to the former case. Moreover, the

inverse variance increases slowly but progressively with g for PGg^{free}, indicating that compression and elongation movements become more difficult. In contrast, the inverse variance decreases with increasing g for PGg^{mica}. On the other hand, $(L_{ee}/R_g)^2$= 12 for rigid macromolecules, where R_g is the radius of gyration. For PGg^{free} and PGg^{mica} the relative deviation of $(L_{ee}/R_g)^2$ from 12 is around 2% and 0.5%, respectively (Table S1). This behavior is fully consistent with the fact that the inverse variance of L_{ee} is higher for PGg^{mica} than for PGg^{free}.

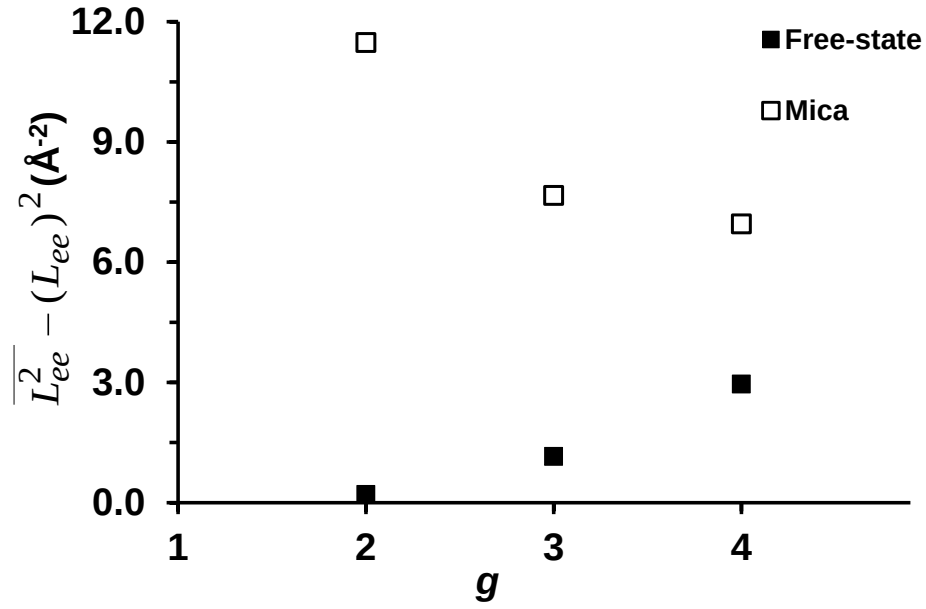

Figure 7. Size dependence of the inverse variance of the L_{ee} for PGg^{free} and PGg^{mica}**.**

CONCLUSIONS

The molecular object behavior of DPs made of a poly(methacrylic acid) backbone and dendrons containing both amide and aromatic groups, which are among the most studied in the field,[2-5,14-16] has been examined using MD simulations. Results reveal that an attractive mica surface induces only a moderate flattening of DPs during an adsorption process, while their widths and densities remain basically unaffected. This is

particularly evident by comparing the variation of the height free PG4 upon adsorption onto mica with that obtained for the poly(amidoamine) dendrimer of g= 4,[25] which is practically identical in terms of chemical constitution. Accordingly, the height of PG4 decreases ~20% upon adsorption while that of the dendrimer reduces by more than 100%, reflecting the behavior of DPs as single molecular objects. Furthermore, although the loss of the cross-section circularity observed in DPs grows with increasing g for the investigated range of g, this effect is not only due to the reduction of the cross-sectional height but to small protuberances whose frequency grows with the radius of the DP. This loss with increasing g deserves further comment because it is expected that when g approaches the maximum generation (g_{max}), the ability of DPs to flatten should become minimal. A comparison of the theoretical minimum and maximum diameters of DPs, however, offers an explanation for this seeming contradiction. While for low as well as for generations near g_{max} these diameters are very similar, for intermediate generations they exhibit a maximum difference. For the DPs investigated in the present study the maximum difference is in fact expected for g=4 where the largest flattening was found. If this interpretation holds true, MD simulations on higher generation polymers of the same kind should result in less flattening. This work is in progress. Overall, the reversible structural changes are too minor to significantly alter the cylindrical shape of these macromolecules. Thus, their persistent shape qualifies such macromolecules as molecular objects.

ACKNOWLEDGEMENTS

This work was supported by MICINN-FEDER funds (MAT2012-34498) the Generalitat de Catalunya (2009SGR925 and XRQTC) and CESCA. Authors are indebted to Dr. Hendrik Heinz, who kindly supplied the mica super cell model.

SUPPORTING INFORMATION

Structural parameters, surface-PG*g* interaction energies, density profiles for PGg^{free}, and additional representative solid images of the cross-sections. This material is available free of charge via the Internet at http://pubs.acs.org.

REFERENCES

1. Schlüter, A. D.; Rabe J. P. Dendronized Polymers: Synthesis, Characterization, Assembly at Interfaces, and Manipulation. *Angew. Chem. Int. Ed. Engl.* **2000**, *39*, 864-883.
2. Guo, Y.; van Beek, J. D; Zhang, B.; Colussi, M.; Walde, P.; Zhang, A.; Kröger, M.; Halperin, A.; Schlüter, A. D. Tuning Polymer Thickness: Synthesis and Scaling Theory of Homologous Series of Dendronized Polymers. *J. Am. Chem. Soc.* **2009**, *131*, 11841.
3. Zhang, B.; Wepf, R.; Fischer, K.; Schmidt, M.; Besse, S.; Lindner, P.; King, B. T.; Sigel, R.; Schurtenberger, P.; Talmon, Y.; Ding, Y.; Kröger, M.; Halperin, A.; Schlüter, A. D. The Largest Synthetic Structure with Molecular Precision: Towards a Molecular Object. *Angew. Chem. Int. Ed.* **2011**, *50*, 763-766.
4. Zhang, B.; Wepf, R.; Kröger, M.; Halperin, A.; Schlüter, A. D. Height and Width of Adsorbed Dendronized Polymers: Electron and Atomic Force Microscopy of Homologous Series. *Macromolecules* **2011**, *44*, 6785-6792.
5. Schlüter, A. D.; Halperin, A.; Kröger, M.; Vlassopoulos, D.; Wegner, G.; Zhang, B. Dendronized polymers: Molecular objects between conventional linear polymers and colloidal particles. *ACS Macro Lett.* **2014**, 3, 991-998.

6. Chen, Y.; Xiong, X. Tailoring Dendronized Polymers *Chem. Commun*. **2010**, *46*, 5049-5060.

7. Xiong, X.; Chen, Y.; Feng, S.; Wang, W. Codendronized Polymers: Wormlike Molecular Objects with a Segmented Structure. *Macromolecules* **2007**, *40*, 9084-9093.

8. Khan, A.; Zhang, B.; Schlüter, A. D. "Dendronized Polymers: An Approach to Single Molecular Objects", In "Synthesis of Polymers" (Ed: Schlüter, A. D.; Hawker, C. J.; Sakamoto, J.), Wiley-VCH Verlag GmbH & Co. KGaA Weinheim, Germany, 2012.

9. Frauenrath, H. Dendronized Polymers-Building a New Bridge from Molecules to Nanoscopic Objects. *Prog. Polym. Sci*. **2005**, *30*, 325-384.

10. Fuhrmann, G.; Grotzky, A.; Lukic, R.; Matoori, S.; Luciani, P.; Yu, H.; Zhang, B.; Walde, P.; Schlüter, A. D.; Leroux, J.-C.Sustained Gastrointestinal Activity of Dendronized Polymer–Enzyme Conjugates. *Nature Chem.* **2013**, *5*, 582-589.

11. Liang, C. O.; Helms, B.; Hawker, C. J.; Fréchet, J. M. J. Dendronized Cyclocopolymers with a Radical Gradient of Polarity and Their Use to Catalyze a Difficult Esterification. *Chem. Commun.* **2003**, *20*, 2524-2525.

12. Grotzky, A.; Nauser, T.; Erdogan, H.; Schlüter, A. D.; Walde, P. A Fluorescently Labeled Dendronized Polymer-Enzyme Conjugate Carrying Multiple Copies of Two Different Types of Active Enzymes. *J. Am. Chem. Soc.* **2012**, *134*, 11392-11395.

13. Fornera, S.; Balmer, T. E.; Zhang, B.; Schlüter, A. D.; Walde, P. Immobilization of Peroxidase on SiO_2 Surfaces with the Help of a

Dendronized Polymer and the Avidin-Biotin System. *Macromol. Biosci.* **2011**, *11*, 1052-1067.

14. Bertran, O.; Zhang, B. Z.; Schlüter, A. D.; Halperin, A.; Kröger, M.; Aleman, C. Computer Simulations of Dendronized Polymers: Organization and Characterization at the Atomistic Level. *RSC Adv.* **2013**, *3*, 126-140.
15. Bertran, O.; Zhang, B.; Schlüter, A. D.; Kröger, M.; Alemán, C. Computer Simulation of Fifth Generation Dendronized Polymers: Impact of Charge on Internal Organization. *J. Phys. Chem. B* **2013**, *117*, 6007.
16. Córdova-Mateo, E.; Bertran, O.; Zhang, B.; Vlassopoulos, D.; Pasquino, R.; Schlüter, A. D.; Kröger, M.; Alemán, C. Interactions in Dendronized Polymers: Intramolecular Dominates Intermolecular. *Soft Matter* **2014**, *10*, 1032-1044.
17. Bertran, O.; Curcó, D.; Zanuy, D.; Alemán, C. Atomistic Organization and Characterization of Tube-Like Assemblies Comprising Peptide-Polymer Conjugates: Computer Simulation Studies. *Faraday Discuss.* **2013**, *166*, 59-82.
18. Phillips, J. C.; Braun, R.; Wang, W.; Gumbart, J.; Tajkhorshid, E.; Villa, E.; Chipot, C.; Skeel, R. D.; Kale, L.; Schulten, K. Scalable Molecular Dynamics with NAMD. *J. Comput. Chem*. **2005**, *26*, 1781-1802.
19. Cornell, W. D.; Cieplak, P.; Bayly, C. I.; Gould, I. R.; Merz, K. M.; Ferguson, D. M.; Spellmeyer, D. C.; Fox, T.; Caldwell, J. W.; Kollman, P. A. A Second Generation Force Field for the Simulation of Proteins, Nucleic Acids, and Organic Molecules. *J. Am. Chem. Soc.* **1995**, *117*, 5179-5197.
20. Wang, J.; Wolf, R. M.; Caldwell, J. W.; Case, D. A. Development and Testing of a General Amber Force Field. *J. Comput. Chem.* **2004**, *15*, 1157-1174.

21. Heinz, H.; Koerner, H.; Anderson, K. L.; Vaia, R. A.; Farmer, B. L. Force Field for Mica-Type Silicates and Dynamics of Octadecylammonium Chains Grafted to Montmorillonite. *Chem. Mater* **2005**, *17*, 5658-5669.

22. Rothbauer, R. Untersuchung Eines 2M1-Muskovits mit Neutronenstrahlen. *Neues Jahrb. Mineral., Monatsh.* **1971**, 143-154.

23. Toukmaji, A.; Sagui, C.; Board, J.; Darden, T. Efficient Particle-Mesh Ewald Based Approach to Fixed and Induced Dipolar Interactions. *J. Chem. Phys.* **2000**, *113*, 10913-10927.

24. Ryckaert, J. P.; Ciccotti, G.; Berendsen, H. J. C. Numerical Integration of the Cartesian Equations of Motion of a System with Constraints: Molecular Dynamics of n-alkanes. *J. Comput. Phys.* **1977**, *23*, 327-341.

25. Mecke, A.; Lee, I.; Baker jr., J. R.; Banaszak Holl, M. M.; Orr, B. G. Deformability of Poly(amideamine) Dendrimers. *Eur. Phys. J. E* **2004**, *14*, 7-16.

26. Mansfield, M. L. Surface Adsorption on Model Dendrimers. *Polymer* **1996**, *37*, 3835-3841.

27. Takada, K.; Diaz, D. J.; Abruña, H. D.; Cuadrado, I.; Casado, C.; Alonso, B.; Morán, M.; Losada, J. Redox-Active Ferrocenyl Dendrimers: Thermodynamics and Kinetics of Adsorption, In-Situ Electrochemical Quartz Crystal Microbalance Study of the Redox Process and Tapping Mode AFM Imaging. *J. Am. Chem. Soc.* **1997**, *119*, 10763-10773.

28. Tokuhisa, H.; Zhao, M.; Baker, L. A.; Phan, V. T.; Dermody, D. L.; Garcia, M. E.; Peez, R. F.; Crooks, R. M.; Mayer, T. M. Preparation and Characterization of Dendrimer Monolayers and Dendrimer−Alkanethiol

Mixed Monolayers Adsorbed to Gold. *J. Am. Chem. Soc.* **1998**, **120**, 4492-4501.

29. Schlapak, R.; Armitage, D.; Saucedo-Zeni, N.; Latini, G.; Gruber, H. J.; Mesquida, P.; Samotskaya, Y.; Hohage, M.; Cacialli, F.; Howorka, S. Preparation and Characterization of Dense Films of Poly(amidoamine) Dendrimers on Indium Tin Oxide. *Langmuir* **2007**, *23*, 8916-8924.
30. Jachimska, B.; Lapcz ska, M.; Zapotoczny, S. Reversible Swelling Process of Sixth-Generation Poly(amido amine) Dendrimers Molecule As Determined by Quartz Crystal Microbalance Technique. *J. Phys. Chem. C* **2013**, 117, 1136-1145.
31. Boris, D.; Rubinstein, M. A Self Consistent Mean Field Model of a Starburst Dendrimer: Dense Core vs Dense Shell. *Macromolecules* **1996**, *29*, 7251-7260.

TOC